ISSN 1674-1056
http://cpb.iphy.ac.cn
http://iopscience.iop.org/cpb
中国物理 B
Chinese Physics
中国物理 Chinese Physics B

Large-area fabrication: The next target of perovskite light-emitting diodes

Hang Su(苏杭), Kun Zhu(朱坤), Jing Qin(钦敬), Mengyao Li(李梦瑶), Yulin Zuo(左郁琳), Yunzheng Wang(王允正), Yinggang Wu(吴迎港), Jiawei Cao(曹佳维), and Guolong Li(李国龙)

Citation: Chin. Phys. B, 2021, 30 (**8**): 088502. DOI: 10.1088/1674-1056/ac05a4
Journal homepage: http://cpb.iphy.ac.cn; http://iopscience.iop.org/cpb

What follows is a list of articles you may be interested in

Performance and stability-enhanced inorganic perovskite light-emitting devices by employing triton X-100

Ao Chen(陈翱), Peng Wang(王鹏), Tao Lin(林涛), Ran Liu(刘然), Bo Liu(刘波), Quan-Jun Li(李全军), and Bing-Bing Liu(刘冰冰)
Chin. Phys. B, 2021, 30 (**4**): 048506. DOI: 10.1088/1674-1056/abcf47

Reliability of organic light-emitting diodes in low-temperature environment

Saihu Pan(潘赛虎), Zhiqiang Zhu(朱志强), Kangping Liu(刘康平), Hang Yu(于航), Yingjie Liao(廖英杰), Bin Wei(魏斌), Redouane Borsali, and Kunping Guo(郭坤平)
Chin. Phys. B, 2020, 29 (**12**): 128503. DOI: 10.1088/1674-1056/abc154

Stackable luminescent device integrating blue light emitting diode with red organic light emitting diode

Kang Su(苏康), Jing Li(李璟), Chang Ge(葛畅), Xing-Dong Lu(陆兴东), Zhi-Cong Li(李志聪), Guo-Hong Wang(王国宏), Jin-Min Li(李晋闽)
Chin. Phys. B, 2020, 29 (**4**): 048504. DOI: 10.1088/1674-1056/ab77ff

Infrared light-emitting diodes based on colloidal PbSe/PbS core/shell nanocrystals

Byung-Ryool Hyun, Mikita Marus, Huaying Zhong(钟华英), Depeng Li(李德鹏), Haochen Liu(刘皓宸), Yue Xie(谢阅), Weon-kyu Koh, Bing Xu(徐冰), Yanjun Liu(刘言军), Xiao Wei Sun(孙小卫)
Chin. Phys. B, 2020, 29 (**1**): 018503. DOI: 10.1088/1674-1056/ab5fb7

Enhanced performance of AlGaN-based ultraviolet light-emitting diodes with linearly graded AlGaN inserting layer in electron blocking layer

Guang Li(李光), Lin-Yuan Wang(王林媛), Wei-Dong Song(宋伟东), Jian Jiang(姜健), Xing-Jun Luo(罗幸君), Jia-Qi Guo(郭佳琦), Long-Fei He(贺龙飞), Kang Zhang(张康), Qi-Bao Wu(吴启保), Shu-Ti Li(李述体)
Chin. Phys. B, 2019, 28 (**5**): 058502. DOI: 10.1088/1674-1056/28/5/058502

REVIEW

Large-area fabrication: The next target of perovskite light-emitting diodes*

Hang Su(苏杭)[1], Kun Zhu(朱坤)[1], Jing Qin(钦敬)[1], Mengyao Li(李梦瑶)[1], Yulin Zuo(左郁琳)[1], Yunzheng Wang(王允正)[1], Yinggang Wu(吴迎港)[1], Jiawei Cao(曹佳维)[2], and Guolong Li(李国龙)[1,†]

[1] *Key Laboratory of Photovoltaic Materials, Ningxia University, Yinchuan* 750000, *China*
[2] *Advanced Computer Science, University of Leeds, Leeds LS2 9JT, UK*

(Received 6 April 2021; revised manuscript received 6 May 2021; accepted manuscript online 27 May 2021)

Perovskite materials show exciting potential for light-emitting diodes (LEDs) owing to their intrinsically high photoluminescence efficiency and color purity. The research focusing on perovskite light-emitting diodes (PeLEDs) has experienced an exponential growth in the past six years. The maximum external quantum efficiency of red, green, and blue PeLEDs has surpassed 20%, 20%, and 10%, respectively. Nevertheless, the current PeLEDs are still in the laboratory stage, and the key for further development of PeLEDs is large-area fabrication. In this paper, we briefly discuss the similarities and differences between manufacturing high-quality and large-area PeLEDs and perovskite solar cells. Especially, the general technologies for fabricating large-area perovskite films are also introduced. The effect of charge transport layers and electrodes on large-area devices are discussed as well. Most importantly, we summarize the advances of large-area (active area ≥ 30 mm^2) PeLEDs reported since 2017, and describe the methods for optimizing large-area PeLEDs reported in the literature. Finally, the development perspective of PeLEDs is presented for the goal of highly efficient and large-area PeLED fabrication. It is of great significance for the application of PeLEDs in future display and lighting.

Keywords: perovskite light-emitting diodes, large-area fabrication, film optimization, manufacture technologies

PACS: 85.60.Jb, 81.07.Pr, 81.10.Dn **DOI:** 10.1088/1674-1056/ac05a4

1. Introduction

Metal halide perovskite (MHP) materials have undergone remarkable development in the field of light-emitting diodes (LEDs) owing to their outstanding optical and electrical properties. MHP materials are semiconducting materials that have an ABX_3 perovskite crystal structure, in which A is an organic cation (*e.g.*, MA^+, FA^+) or an alkali-metal cation (*e.g.*, Cs^+ or K^+), B is a transition-metal cation (*e.g.*, Pb^{2+}, Sn^{2+}), and X is a halide anion (Cl^-, Br^-, I^-).[1–8] The MHP materials are suitable for the emission layer in LEDs due to their properties of high color purity (full width at half maximum < 20 nm), low material cost, high photoluminescence quantum yield (PLQY), high charge-carrier mobility, and solution processability.[9–12] Furthermore the emitting color can be varied by alternating the halide anion of MHP materials from Cl^- to Br^- or I^-[13] which indicates that these materials have potential to fabricate the white-color LEDs. Therefore, MHP materials are promising materials for future large-area display and lighting.

As shown in Fig. 1(a), the structure of perovskite light-emitting diodes (PeLEDs) is similar to that of the organic LEDs. PeLEDs are composed of the layers of anode, cathode, hole transport layer (HTL), perovskite emission layer, and electron transport layer (ETL). As a bias voltage is applied, electrons and holes are injected from the cathode and anode respectively. The charges recombine in the perovskite layer and produce photons by radiative recombination, as presented in Fig. 1(b). The crucial parameters that determine the performance of PeLEDs cover the maximum luminance, the current efficiency (CE), the external quantum efficiency (EQE), and the stability. The CE and EQE are calculated according to Eqs. (1) and (2)

$$\mathrm{CE} = \frac{L}{J}, \tag{1}$$

where L is the luminance of the PeLEDs, and J is the current density.

$$\mathrm{EQE} = \mathrm{IQE} \cdot \eta = \frac{N_\mathrm{p}}{N_\mathrm{e}}, \tag{2}$$

where IQE is the internal quantum efficiency of the PeLEDs, η is the efficiency of photons emitted into space, N_p is the number of photons emitted into space, and N_e is the number of electrons injected into PeLEDs.

In 2014, Tan *et al*. first reported green and red PeLEDs at room temperature, but the maximum EQE of PeLEDs was less than 1%.[14] With efforts made over the last seven years, the blue PeLEDs achieved the recorded EQE of 11%.[15] At present, the best recorded EQE for green, red, and

*Project supported by the Ningxia Key Project of Research and Development Plan (Grant No. 2020BDE03013).
†Corresponding author. E-mail: liglo@163.com
© 2021 Chinese Physical Society and IOP Publishing Ltd

near-infrared (NIR) devices are 20.3%, 21.3%, and 21.6%, respectively.[16–18] Although the high efficiency of PeLEDs has been successfully demonstrated, the active-area of devices is still on the order of a few square millimeters. In addition, PeLEDs present a broad performance variation in different areas of the devices. As such, the present goal for PeLEDs is aiming at large-area fabrication.

High-efficiency, stability, and large-area fabrication are the key to manufacture PeLEDs commercially. At present, some groups have focused on the efficiency and stability of PeLEDs and made great progress.[19–22] As for large-area PeLEDs, special challenges are required to be overcome. Primarily, the kinetics of perovskite crystal growth is under consideration for well-controlling the solution process of large-area perovskite films. The literatures have reported that the enlarged perovskite grains unavoidably increases the density of pinholes in perovskite film, which leads to the rising leakage current of PeLEDs.[23] Secondly, it is unclear how to improve the luminance uniformity while enhancing the carrier injection level of PeLEDs. Apparently, the injection levels for different regions are remarkably different as the PeLEDs are enlarged. To obtain a uniform brightness of large-area PeLEDs, the homogeneous charge transport layers (CTLs) act as importantly as the perovskite film. Thirdly, the enhanced efficiency of large-area PeLEDs remains an important issue. For the large-area devices, the decreased EQE can be attributed to the enhancement in defect-induced high non-radiative recombination and the complex photon losses inside the device as well.[24] In addition, the device stability is another interesting topic for large-area PeLEDs. In previous studies, Lee and co-workers discussed the origins of the low stability of PeLEDs and adopted the strategies to improve the stability of MHP materials and PeLEDs.[25] Rogach and co-workers summarized the basic characteristics of MHP materials and PeLEDs, and put forward the methods for improving the efficiency of PeLEDs.[26] Although it did not cover the large-area PeLEDs, their researches undeniably provided the novel viewpoints for the fabrication of large-area PeLEDs.

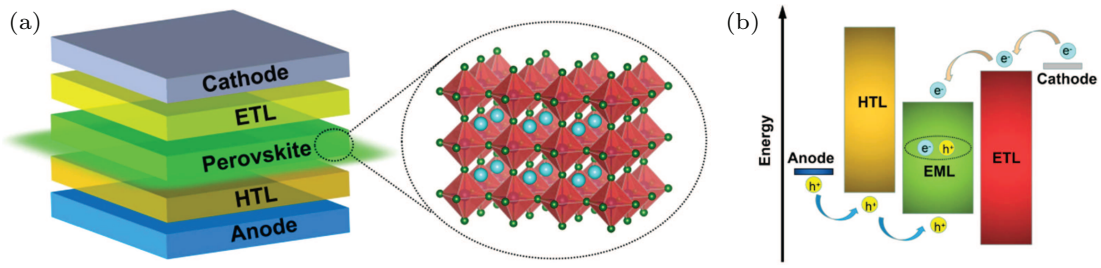


Fig. 1. (a) The device structure of a PeLED; (b) the radiative recombination of electrons and holes.

Here, we briefly discuss the similarities and differences between large-area PeLEDs and perovskite solar cells (PeSCs), and introduce the methods for obtaining large-area emission films. Further, we illustrate the effect of CTLs and electrodes on the large-area PeLEDs. Hereafter, the recent advances of large-area PeLEDs (active area ≥ 30 mm^2) are presented, and the methods for optimizing large-area PeLEDs are summarized. Finally, a prospective development of PeLEDs is given in this paper.

2. Similarities and differences between large-area PeSCs and PeLEDs

At present, PeSCs not only demonstrate high power conversion efficiency, but also make satisfactory progress in large-area fabrication.[27–29] Yan *et al.* and You *et al.* summarized the development of large-area PeSCs in recent years.[30,31] Inspired by this, it is also desirable to fabricate large-area PeLEDs. PeSCs and PeLEDs have similar device structure, and many materials in PeSCs can be utilized in PeLEDs. For example, poly(3,4-ethylenedioxythiophene) polystyrene sulfonate (PEDOT:PSS), MoO_3, ZnO, and NiO_x can be used either in PeLEDs or in PeSCs as the charge transport layers. Thereby, the manufacturing technology of charge transport layers in large-area PeSCs can also be employed in large-area PeLEDs. In devices, the carrier transport barriers at interfaces and the defect/trap states at the perovskite grain boundaries are common factors that restrict the performance of PeLEDs and PeSCs. Due to the energy barrier at interfaces severely hindering the transfer efficiency of carrier, it requires a well-matching energy level alignment to reduce the loss of injected charge carriers, which is an effective scheme to improve the device performance of PeLEDs and PeSCs. For PeSCs, electron–hole pairs are generated in the perovskite layer, diffused and separated into the charge carriers, which are collected by two electrodes. However, the defects in the perovskite layer act as the recombination centers, and trap a large number of free carriers, which results in a short decay lifetime and the instability of PeSCs. For PeLEDs, the limited EQE is mainly due to an obvious competition between the defect-states trapping (the first-order decay process) and the slow electron–hole bimolecular radiative recombination (the second-order decay process) under working conditions (Fig. 2(a)).[32] Especially, this effect will be amplified when the density of injected charge carriers is lower than

10^{15} cm^{-3}. The present defect–passivation methods are unavailable in large-area PeLED fabrication. Huang *et al.* recently used surface mechanical peeling to achieve low-cost and large-area passivation of perovskite films.[33] The nanoscratch on original and polished $MAPbI_3$ film characterized the mechanical properties of the surface layer. It proved that the adhesion force of defective surface layer to the region underneath was less than the inside of the crystal grain. The polycrystalline perovskite film exhibits an lattice discontinuity of its surface. The defective surface surrounded by an amorphous phase had stronger dangling chemical bonds and provided the amount of vacancies, which can be mechanically peeled off from the defective surface layer with a low-cost method. The film after tape treatment was smoother, and the obtained super stable PeSCs also proved that the defects were effectively eliminated by the way.

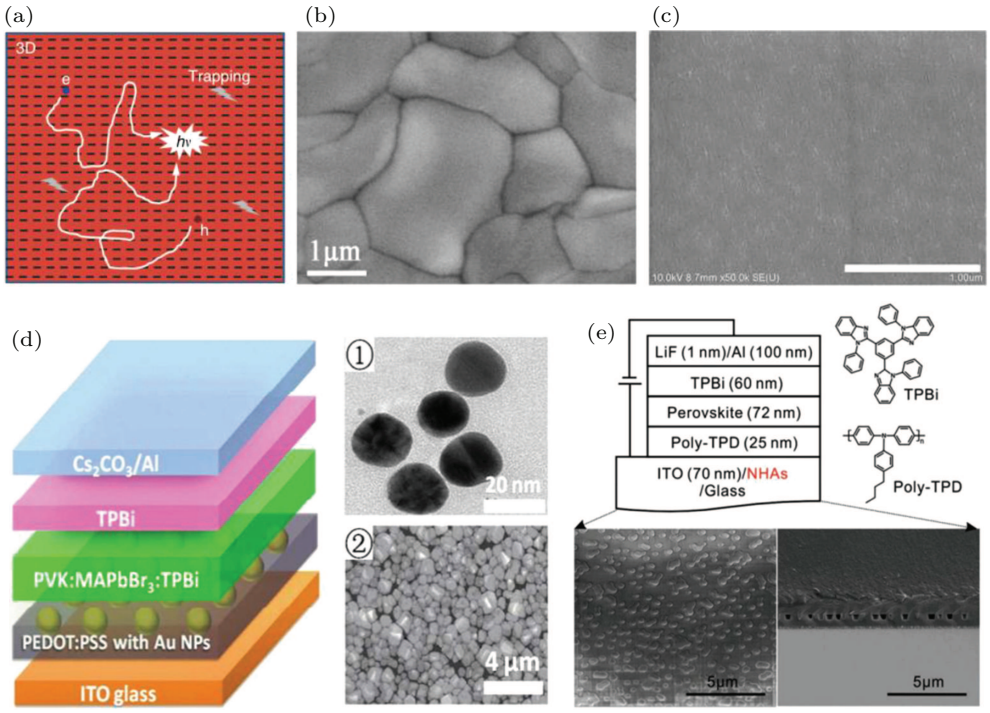


Fig. 2. (a) The trap-assisted recombination and slow bimolecularly radiative recombination in the three-dimensional (3D) perovskite;[32] (b) the scanning electron microscope (SEM) image of perovskite film with large grain in a PeSC;[34] (c) the SEM image of perovskite film with small grain in a PeLED;[35] (d) the structure of the plasmonic PeLEDs incorporating Au nanoparticles in the PEDOT:PSS layer. The illustrations show the high-resolution transmission electron microscopy (TEM) images of the Au nanoparticles and the morphology of perovskite film on the Au nanoparticles modified PEDOT:PSS layer;[40] (e) the structure of PeLEDs with nanohole arrays, molecular structure of transport materials, and SEM images of the structure.[41]

Nevertheless, there are significant differences in fabricating large-area PeLEDs and PeSCs. Compared with PeSCs, PeLEDs require better uniformity of the perovskite layer to prevent the broken-down of perovskite crystals under high bias voltage. A well-controlled crystallization process is essential for perovskite film, which is divided into two steps, namely the nucleation and crystal growth. As the solvent volatilizes during the spin-coating, the solution becomes supersaturated, resulting in the perovskite crystallization. In order to form a compact perovskite film with good coverage, a high nucleation rate is required before the crystals start to grow. Some approaches have been adopted to control this process, such as the antisolvent treatment, solvent annealing treatment and gas-assisted deposition, etc. Although both PeSCs and PeLEDs require high crystallinity and good coverage, the grain sizes for PeSCs and PeLEDs are poles apart. In PeSCs, a flat perovskite film with large-size grains is fabricated to improve the charge transfer efficiency (Fig. 2(b)).[34] In comparison, a smooth perovskite film with small-grains is preferable for PeLEDs to enhance the probability of radiative recombination (Fig. 2(c)).[35] This indicates that the controlled diffusion process that determines crystal growth is different. The crystallization rate of perovskite can be controlled by incorporating additives into the perovskite precursor solution. Snaith *et al.* digged into the perovskite growth kinetics with the incorporation of HBr and HI in the precursor solution.[36] The addition of halogen acid could initiate the dissolution of the lead polyhalide colloid as the nucleation center in the film. The dissolution of the large colloid led to a decrease in the center of the crystal nucleus, which prolonged the growth period of the crystal. The "impurity effect" of molecular additives encourages the formation of large grains by increasing the supersaturation and Gibbs energy for nucleation during a conventional film-forming process, which is unfavorable for the PeLEDs. In order to prevent the crystal coarsening due to the additive, Lee *et al.* employed 2,2',2"-(1,3,5-Benzinetriyl)-

tris(1-phenyl-1-H-benzimidazole) (TPBi) as an additive to deposit perovskite film.[37] Acting as a 'fence', the organic semiconductor hindered the diffusion of the crystal interface. A controllable pinning process induced instantaneous nucleation and a rapid crystal growth by drastically changing the solubility state of the spinning perovskite quasi-film, thus the small grain was formed. The annealing treatments for PeSCs and PeLEDs are totally different. Huang *et al*. annealed the perovskite film in a dimethylformamide (DMF) atmosphere.[38] The solvent vapor re-wetted the perovskite material, which promoted the precursor material to continue to diffuse in the wet perovskite film, thus inducing the grain growth. Sun *et al*. used chloroform, which has a lower polarity than DMF, to combine the chloroform atmosphere treatment with the annealing process of the perovskite film. The treated PeLEDs showed surprising working stability and high efficiency.[39] In addition, the theoretical investigation implies that a promising perovskite absorber should exhibit high electronic dimensionality. The slow free electron–hole bimolecular radiative recombination and low exciton binding energy in these three-dimensional (3D) MHP materials spur efficient photovoltaic operation. In PeLEDs, high exciton binding energy and quantum confinement effect are beneficial to accelerate radiative recombination in the emission layer, utilizing low-dimensional materials, *e.g*., quantum dots (QDs), two-dimensional (2D) perovskite, quasi-2D perovskite quantum wells, is feasible to improve the exciton binding energy of PeLEDs. The light-trapping led by the high refractive difference between layers of the device results in poor performance, which severely restricts the EQE of PeLEDs. Doubtlessly, this effect will be magnified in large-area PeLEDs. In recent years, some researchers have been interested in promoting the light extraction efficiency of PeLEDs. As the small-area device is concerned, the enhancement of light out-coupling efficiency can be achieved by introducing plasma resonance to redistribute the optical field or by inserting the micro-nano optical structure into the device to realize the optimization of light propagation path (Figs. 2(d) and 2(e)).[40,41] However, how to apply these methods to large-area devices is still under investigation.

3. Technologies for fabricating large-area perovskite layer

So far, researchers adopt some strategies to obtain high-quality perovskite films. Spin-coating is widely used to fabricate high-efficiency PeLEDs, and the thickness of perovskite film can be well-controlled by varying the rotation speed and solution concentration.[42–44] Figure 3 presents the processes of fabricating perovskite films by one-step and two-step spin-coating methods.[45] In one-step process, the anti-solvent dripping method is constantly employed to realize the process of rapid and uniform nucleation by reducing the residue of precursor solvents such as DMF and dimethyl sulfoxide (DMSO), resulting in a smooth and uniform perovskite film.[46]

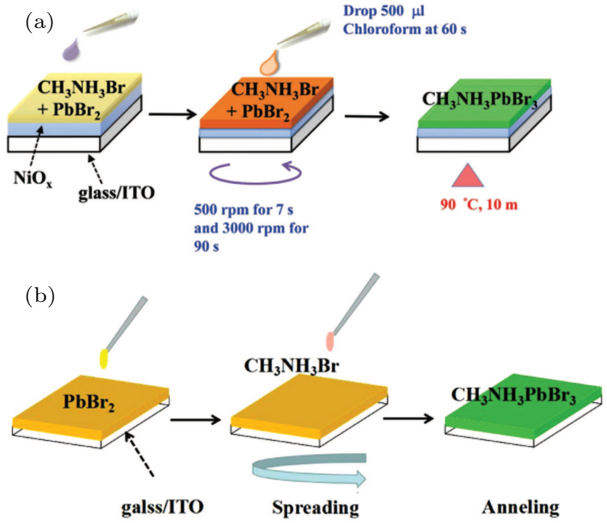


Fig. 3. (a) One-step spin coating method;[45] (b) two-step spin coating method.

In 2018, Sun *et al*. realized the control and optimization of perovskite grain size and film morphology by doping PEABr. They further suppressed the crystallization of the PEABr phase and optimized the domain size and distribution. Thus, a well-controlled phase separation was obtained between the organic and inorganic phase by incorporating a small concentration of an organic molecule 1,4,7,10,13,16-hexaoxacyclooctadecane as an additive. Finally, a PeLED with a maximum EQE of 15.5% was achieved through one-step spin-coating method. Furthermore, a large-area PeLED with a size of 150 mm^2 exhibited a bright and uniform lighting.[47] In the same year, Wei and co-workers also employed one-step spin-coating method to fabricate a bright and homogeneous large-area PeLED with size of 120 mm^2. Concerning the difference of the solubility and crystallinity between the perovskite emission material ($CsPbBr_3$) and passivation agent (MABr) in polar solvents, a perovskite layer with graded composition based on a quasi-core/shell structure was fabricated, resulting in a combination of defect-passivation and balanced charge injection. Moreover, the charge injection balance of the device was improved by inserting a polymethylmethacrylate (PMMA) insulating layer between the perovskite layer and the ETL, thereby reaching a record EQE of 20.3%.[16] In 2019, Tang's team employed the one-step spin coating method to obtain a super large-area green PeLED with 1225 mm^2, which showed incredible brightness and emission uniformity (Fig. 4(a)).[48] Unfortunately, the luminance and efficiency values of the devices were not mentioned in the references.

Concerning the spin-coating, the perovskite utilization ratio should be improved if it is applied in commercial manufacture of PeLEDs. Besides, the traditional anti-solvents, such

as chlorobenzene, toluene, and chloroform, are unfriendly to the environment. During spin-coating process, the dripping behavior of anti-solvent easily influences the perovskite morphology, which leads to the low uniformity of perovskite film, thus deteriorates the performance of the devices. Moreover, low reproducibility of the devices can be attributed to inhomogeneous nucleation of the perovskite. All of these properties are undesirable for manufacturing a pinhole-free and uniform large-area perovskite film. Thereby, some other methods are employed to prepare a high-quality large-area emission layer. For example, chemical vapor deposition (CVD) is a promising alternative due to its ability to batch process and the potential for homogeneous large-area deposition. In 2017, Qi and co-workers deposited $PbBr_2$ on MABr to synthesized $MAPbBr_3$ by CVD (Fig. 4(b)).[49] Similarly, Tang *et al.* and Bi *et al.* used vacuum-deposited and thermal evaporation deposition to fabricate PeLEDs, respectively (Fig. 4(c)).[50,51] However, the high performance could not be acquired for large-area PeLEDs, the brightness of large-area PeLEDs was only hundreds of $cd{\cdot}m^{-2}$. Moreover, the continuous vacuuming process also caused an increase in manufacturing costs. Slot-die coating is previously adopted to make efficient organic LEDs because of taking advantages in saving materials, easy fabrication, and as a result of lower production costs.[52,53] Gas quenching is a technique that induces rapid crystallization of perovskite film by directly blowing N_2 to the substrate. In 2019, Bolink *et al.* took this strategy to upscale PeLEDs to area of 230 cm^2 by developing a protocol for slot-die coating combined with gas quenching (Figs. 4(d) and 4(e)). The integrated large-area devices (446 $mm^2\times$ 9) with three slot-die coated layers exhibited uniform emission with a peak luminance of 550 $cd{\cdot}m^{-2}$ and a maximum CE of 2.6 $cd{\cdot}A^{-1}$.[54] Yu *et al.* employed the fully printing method to manufacture PeLEDs, which is also a potential technique to fabricate large-area perovskite films (Fig. 4(f)).[55] In addition, methods for fabricating large-area PeSCs, such as spray coating and inkjet printing, are worth of exploration as well. Spraying is a low-temperature coating technology, which is widely used in industry because of the advantages of low cost, large-scale, rapid manufacturing and high material utilization. The process of the spray-coating is shown in Fig. 5(a).[56] The perovskite precursor is sucked out from the container and converted into perovskite droplets. Then, the mist-like perovskite adheres to the substrate and coalesces into a wet film, followed by annealing to obtain a smooth perovskite layer. The working principle of inkjet printing is that raw materials are ejected from nozzles in the form of droplets and accurately deposited on the substrate. Continuous inkjet printing is followed by drop-on-demand inkjet printing (Figs. 5(b) and 5(c)).[57] It can be expected that this method will become a rising star in the field of large-area PeLEDs due to low material consumption and easy large-area production.

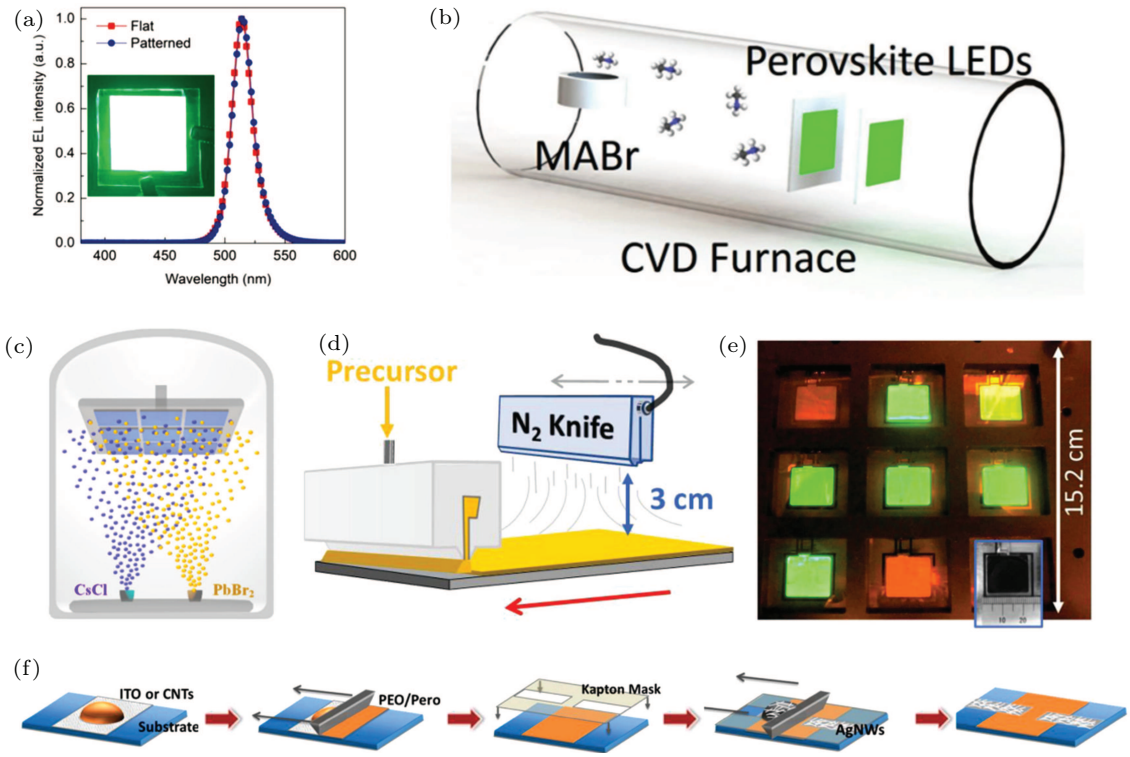


Fig. 4. (a) A large-area green PeLED with 3.5 cm×3.5 cm and electroluminescence (EL) spectrum;[48] (b) schematic diagram of depositing MABr onto $PbBr_2$ to form $MAPbBr_3$ by CVD;[49] (c) schematic illustration of manufacturing perovskite film by dual-source co-evaporation;[50] (d) the slot-die coating process combined with gas quenching for preparing perovskite film;[54] (e) photograph of the light output from the operational PeLEDs (6 devices in ON state) from a slot-die coated substrate;[54] (f) schematic of printing a PeLED.[55]

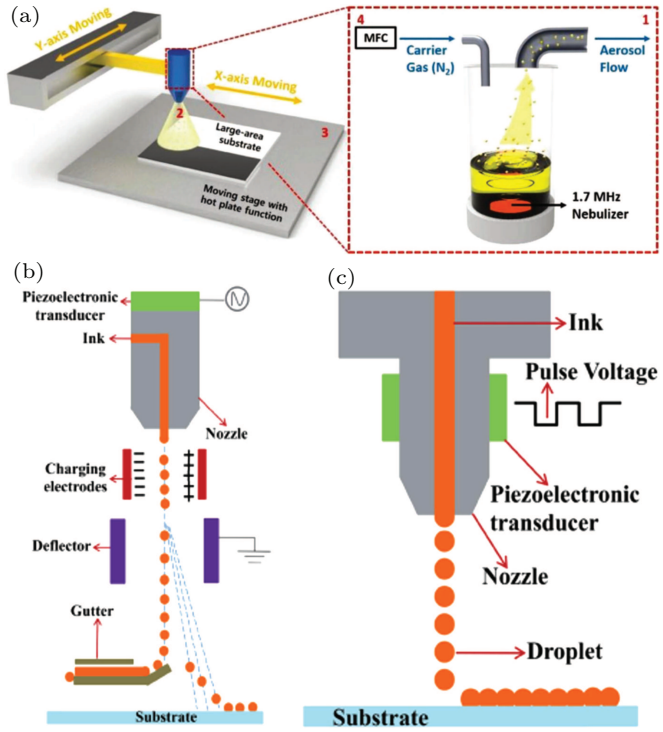


Fig. 5. (a) Schematic representation of the spray-coating process;[56] (b) continuous inkjet printing; [57] (c) drop-on-demand inkjet printing.[57]

4. The effect of CTLs and electrodes on large-area PeLEDs

Device structure is essential for PeLEDs. An appropriate structure facilitates the injection, transportation, and recombination of the carrier in the perovskite emission layer, and it balances the distribution of charge carriers, thus improves the efficiency of exciton radiative recombination. It is well known that the growth and crystallization of perovskite film are remarkably affected by the substrate. Meanwhile, a suitable optical matching interface enhances CE of the PeLEDs, so the interlayer engineering plays an important role in improving the performance of PeLEDs.[58,59] The uniform brightness of large-area PeLEDs depends on a smooth and uniform emission layer, the high-quality CTLs are also indispensable in large-area PeLEDs. In order to achieve homogeneous luminance in large-area devices, it is expected to keep a balance of charge injection from the CTLs to emission layer. In fact, an imbalanced charge injection easily arouses the local hot-spots, the leakage current can also be attributed to the discontinuous CTLs. As such, a poor formation of the CTLs severely affects the morphology of the large-area emission layer, thus results in a poor performance of large-area PeLEDs. Song and coworkers employed poly(9-vinylcarbazole) (PVK) as an interlayer while fabricating a 1280-mm^2-area PeLED.[60] In order to improve the poor morphology of the hydrophobic layer of PVK, a hot casting method was adopted to pretreat the substrate before spin-coating the perovskite precursor solution. As the casting temperature was rising up to 100 °C, a pinhole-free and smooth perovskite film was achieved.

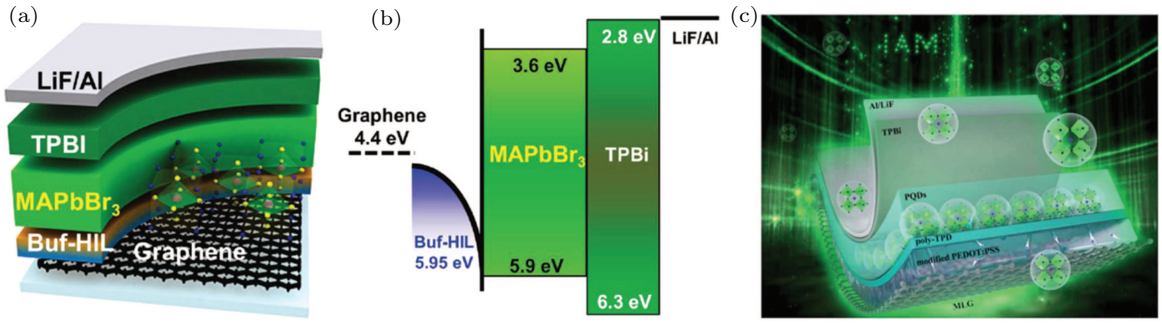


Fig. 6. (a) Device structure of PeLED with graphene electrode and $MAPbBr_3$ emitter;[62] (b) energy band structure of the PeLED;[62] (c) diagram of the QDs PeLED fabricated on graphene.[63]

The active area of PeLEDs is defined by the overlapping zone between the transparent anode and metal cathode layers. Limited by the conductivity of the transparent anode, the injected charges from the edge of the PeLEDs have difficulties in diffusing into its central region as the size of device is amplified. Thus, the brightness in light-emitting zone becomes non-uniform. As the luminous intensity increases, the uneven distribution of brightness becomes distinguishable. Graphene is a promising alternative material in large-area transparent electrodes, and becomes a rising star due to its extraordinary properties, including good conductivity (106 s·m^{-1}), high optical transmittance (97.7%), and high intrinsic charge carrier mobility (2×10^5 cm^2·V^{-1}·s^{-1}).[61] In 2017, Lee *et al.* first demonstrated an efficient flexible PeLED based on the graphene anode and a self-organized gradient buffer hole-injection layer (Figs. 6(a) and 6(b)). A maximum luminance over 10000 cd·m^{-2} and a high efficiency of $CE_{max} = 18.0$ cd·A^{-1} were achieved.[62] In addition, Huang *et al.* successfully fabricated a green graphene-based PeLED (Fig. 6(c)), in which PEDOT:PSS was modified by Triton X-100 and DMSO.[63] In recent years, great progress is made on the basis of graphene, but there still exist some problems. For example, when it is prepared by chemical methods, graphene oxide cannot be fully reduced due to the limitation of the sub-

strate and reaction conditions. Therefore, there is still a long way to realize the industrial application of graphene in this field. But it is undeniable that graphene gives another choice for PeLEDs' application in large-area display and lighting. Thermal evaporation deposition is usually employed to manufacture metal electrodes. The vacuum deposition indicates a high manufacturing cost, and the emission layer is so fragile that a local leakage current arising from a slight unevenness will deteriorate PeLEDs. Therefore, a large-area uniform metal cathode is required in process of fabricating PeLEDs, which increases the complexity of the manufacturing process. To tackle, a feasible strategy is to realize the interconnections between the sub-PeLEDs inside the device, which significantly improves the luminance uniformity. Certainly, a rising price brought by the adding complexity of device is also noteworthy.[64]

5. Manufacturing the high-efficiency large-area PeLEDs

There are many factors that affect the performance of PeLEDs, such as film quality, grain size, material composition, surface and interface defects, energy level matching and photon emission loss. In recent years, the performance of PeLEDs is mainly improved through appropriate modification of perovskite materials by doping and surface passivation, as well as the improvements of the device structure including interface engineering, improvement of the photon emission by plasmonic enhancement and choice of suitable CTLs.[65] Although there are some special challenges in fabricating large-area devices, these optimization strategies are still suitable for improving the performance of large-area PeLEDs. Researchers have begun to explore the fabrication of high-efficiency large-area PeLEDs by these methods. We conduct an exhaustive survey on the large-area (active area ≥ 30 mm^2) PeLEDs reported since 2017 (Table 1).

Table 1. The progress of large-area PeLEDs (active area ≥ 30 mm^2).

Year	Device structure	Emitting materials	Method	Active area (mm^2)	EL (nm)	EQE$_{max}$ (%)	L$_{max}$ (cd·m^{-2})	Ref.
2017	ITO/PFN-OX/Pe/TAPC /MoO_3/Au	$MAPbBr_3$	CVD		540		>100	49
2017	ITO/ZnO/Pe/α-NPD /MoO_3/Al	$Cs_{0.1}(MA_{0.17}FA_{0.83})_{0.9}PbBr_{0.33}I_{2.67}$ $Cs_{0.1}(MA_{0.17}FA_{0.83})_{0.9}PbBr_{2.97}I_{0.03}$	spin coating	100 1 inch (diagonal)	750, 569			66
2017	ITO/PEDOT:PSS/Poly-TPD/Pe/3TPYMB/LiF/Al	$FAPbBr_3$	spin coating	300	530±1	2		67
2018	ITO/Poly-TPD/Pe/TPBi /LiF/Al	PEABr : $CsPbBr_3$	spin coating	150	514			47
2018	ITO/PEDOT:PSS/Pe /B3PYMPM/LiF/Al	$CsPbBr_3$/MABr	spin coating	120	525			16
2018	ITO/PVK/Pe/ TmPyPB/LiF/Al	$(BIZ)_2(FA)_{n-1}Pb_nBr_{3n+1}$	spin coating	49	≈ 535	6.4	27700	68
2018	ITO/PEDOT:PSS/Pe /3TPYMB/LiF/Al	$(C_8H_{17}NH_3)_2[FA_{0.5}MA_{0.5}PbBr_3]_nPbBr_4$	spin coating	400 > 200 (fle.)	528, 528	6.7, 3.1		69
2018	ITO/PEDOT:PSS/PVK/Pe /TPBi/Liq/Al	$CsPbBr_3$	spin coating	400	510	>10	>10000	70
2019	ITO/ZnO/PEDOT:PSS/Pe /TPBi/LiF/Al	$CsPbBr_3$	spin coating	1225	514			48
2019	ITO/PEDOT:PSS/Di-NPB /Pe/BmPyPhB/LiF/Al	$MAPbBr_3$	slot-die coating	446×9	532	CE=2.6cd A^{-1}	550	54
2020	ITO/PEDOT:PSS/Pe/TPBi /LiF/Al	$CsPbBr_3$-PEO-Cs_2CO_3	spin coating	150	516		>10000	71
2020	ITO/NiO_x/PVK/Pe/TPBi /LiF/Al	$(BA)_2Cs_{n-1}Pb_nBr_{3n+1}$	hot casting	126, 1280	≈ 510, ≈ 510	3.6	2400	60
2020	ITO/PEDOT:PSS/ploy-TPD/TBB/Pe/TPBi/LiF/Al	$FAPbBr_3$	spin coating	400	531	16.3		73
2020	ITO/ZnO/PEIE/Pe /Poly-TPD/MoO_x/Al	$FAPbI_3$-5-AVA	spin coating	900, 900 (fle.)	799, 799	12.1, 1	≈ 30, ≈ 0.56 W·Sr^{-1}·m^{-2}	74

In 2017, Nazeeruddin and co-workers fabricated the blue, green and red PeLEDs with high-efficiency by varying the composition of halides. To demonstrate the uniformity of the emission layer, they developed large-area green (1-inch diagonal) and red (100 mm^2) PeLEDs (Fig. 7(a)). Furthermore, they manufactured a large-area (2-inch diagonal, 1 inch = 2.54 cm) flexible green PeLED by using colorless polyimide to prove the versatility of perovskite film. It was the largest area of PeLEDs at that time.[66] In the same year, Chih-Jen Shih *et al*. demonstrated the ultrapure green PeLEDs composed of the colloidal 2D $FAPbBr_3$ hybrid perovskites, with the stacking number of perovskite unit cells to be around 7 to 10. Moreover, 8 wt% of low dielectric constant compound, PMMA was added into the $FAPbBr_3$ col-

loidal solution to achieve the dielectric quantum trap engineering (Fig. 7(b)). The quantum-confined 2D $FAPbBr_3$ perovskites showed a high exciton binding energy of 162 meV, resulting in a high PLQY of 92% in the spin-coated films. They further demonstrated a large-area PeLED with 300 mm^2, which exhibited a high EQE of 2%.[67] Since 2018, there was an upsurge of manufacturing large-area PeLEDs, the EQE of large-area PeLEDs surpassed 10%. Wang *et al.* demonstrated a novel multiple quantum well perovskite, namely, $(BIZ)_2(FA)_{n-1}Pb_nBr_{3n+1}$ (BIZ = benzimidazolium).[68] The rigid BIZ molecules without branched alkyl-chain can significantly reduce the barrier width to 1.4 nm in perovskite quantum wells. In addition, the carrier mobility of the perovskite film increased without affecting the film quality (Fig. 7(c)). They further optimized the constitution of BIZ-based multiple quantum well perovskites, the multiple quantum well perovskite film was fabricated by spin-coating precursor solutions of BIZBr, FABr, and $PbBr_2$ with various molar ratios of 2:1:2, 2:1.8:3, 2:2:3, and 2:3:4, where the PeLED with molar ratio of 2:1.8:3 exhibited high EL. Thus, a high-performed large-area (49 mm^2) green PeLED was achieved, which exhibited a maximum luminance of 27700 $cd{\cdot}m^{-2}$, and a peak EQE of 6.4%. Shih *et al.* demonstrated a high CE and long operational lifetime PeLED, which contained polydisperse colloidal quantum wells of organic-inorganic hybrid perovskites.[69] In this research, perovskite nanoplates with the formula $(C_8H_{17}NH_3)_2[FA_xMA_{1-x}PbBr_3]_nPbBr_4$ were obtained, where n is the stacking number of perovskite unit cells, determining the optical bandgaps of individual nanoplates (Figs. 7(d) and 7(e)). The PeLED structured with $(C_8H_{17}NH_3)_2[FA_xMA_{1-x}PbBr_3]_nPbBr_4$ nanoplates avoided the fundamental restriction of impeded carrier transport and exciton quenching through the nanocrystalline ligand layer. Finally, a large-area (400 mm^2) PeLED was demonstrated with EQE of 6.7% (Fig. 7(f)).

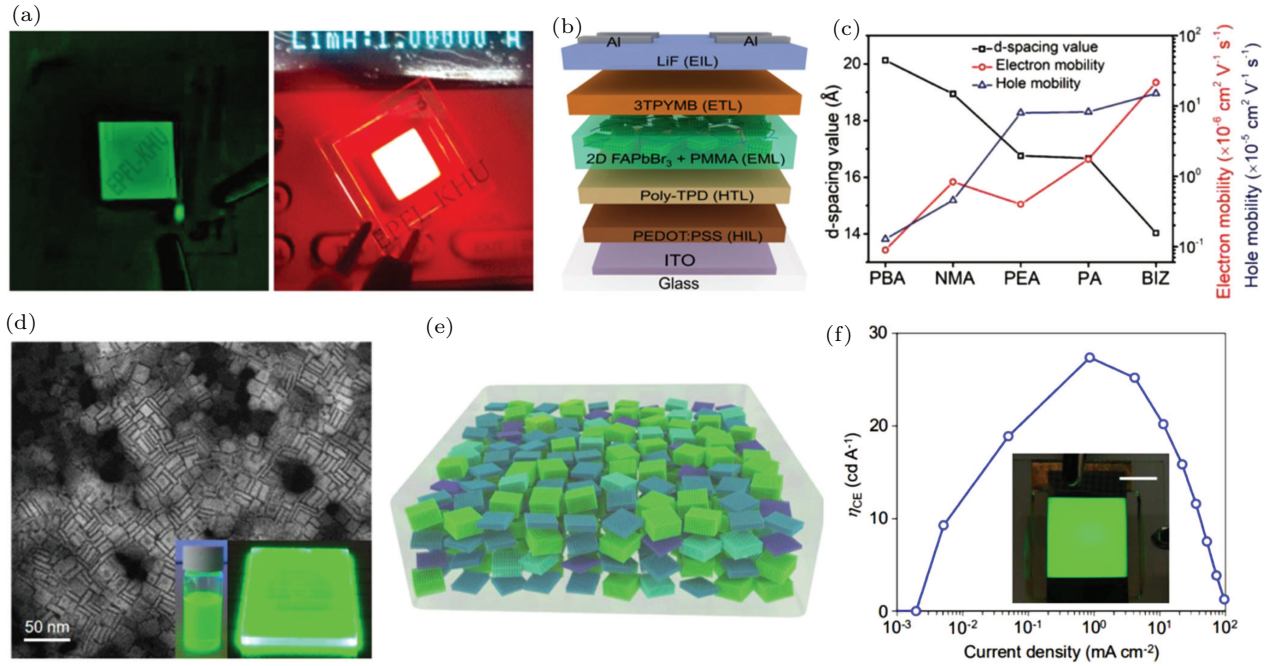


Fig. 7. (a) Picture of large-area devices. Green-colored (1-inch diagonal) and NIR-colored (100 mm^2) PeLEDs operating at 5 V and 8 V, respectively;[66] (b) schematic device architecture of the 2D $FAPbBr_3$-based PeLED;[67] (c) electron and hole mobilities *versus* d-spacing value of $(PBA)_2PbBr_4$, $(NMA)_2PbBr_4$, $(PEA)_2PbBr_4$, $(PA)_2PbBr_4$, and $(BIZ)_2PbBr_4$ perovskite films;[68] (d) representative TEM image and photographs of solution and film under UV excitation;[69] (e) schematic diagram of the superstructure containing randomly stacked nanoplates with different layer numbers;[69] (f) photograph of monochromatic green EL from a large-area PeLED (100 mm^2) and CE in the optimized large-area device.[69]

Liao and co-workers reported an extremely uniform and flat $CsPbBr_3$ film, which was composed of self-assembly core–shell structured quantum dots (SCQDs) with an effective defect-passivation. The core–shell structure of the SCQDs was shown in Fig. 8(a). The formed QDs in a one-step precursor spin-coated $CsPbBr_3$ film were 4.5 nm in average size (Fig. 8(b)), which effectively confined the excited electron–hole pairs in space and led to an ultra-high exciton binding energy of 198 meV. The $CsPbBr_3$ SCQDs film exhibited a high PLQY of 85%. Moreover, a fabrication of relatively large-area (400 mm^2) flexible PeLEDs demonstrated the promising commercial application of $CsPbBr_3$ SCQDs film in multifunctional lighting. The device achieved a brightness of more than 10000 $cd{\cdot}m^{-2}$, and the peak EQE achieved a significant breakthrough of more than 10% (Figs. 8(c) and 8(d)), which represented a milestone progress in the field of large-area PeLEDs.[70] Although the large-area PeLEDs make rapid progress in the EQE and brightness, how to enlarge the effective area of PeLEDs is required to be investigated. Considerable literatures have addressed this issue. Tang *et al.* demon-

strated a 1225-mm^2 large-area PeLED.[48] Besides, Bolink *et al*. reported an area of 446 mm^2 × 9 device by slot-die coating, which had a maximum CE of 2.6 cd·A^{-1}.[54] Maintaining high-efficiency while enlarging PeLEDs seems to be a trade-off. To handle this, some good researches recently pushed the development of large-area PeLEDs to a climax. Zhu *et al*. reported the use of hybrid additives in the $CsPbBr_3$ precursor solution to achieve high-performed large-area PeLEDs by controlling the growth of the emission layer. The hybrid additive comprised a combination of poly ethylene oxide (PEO) and Cs_2CO_3. In Figs. 8(e)–8(h), it can be clearly observed that the hybrid additive having PEO and Cs_2CO_3 was beneficial for improving the morphology of the emission layer, a smooth and dense perovskite film was obtained after doping the hybrid additive. In addition, the hybrid additive not only helped to suppress the leakage current, but also kept the balance of electron–hole current. A 150-mm^2-sized PeLED demonstrated a maximum luminance beyond 10000 cd·m^{-2}, which was more than three times greater than that of a PeLED based on $CsPbBr_3$.[71]

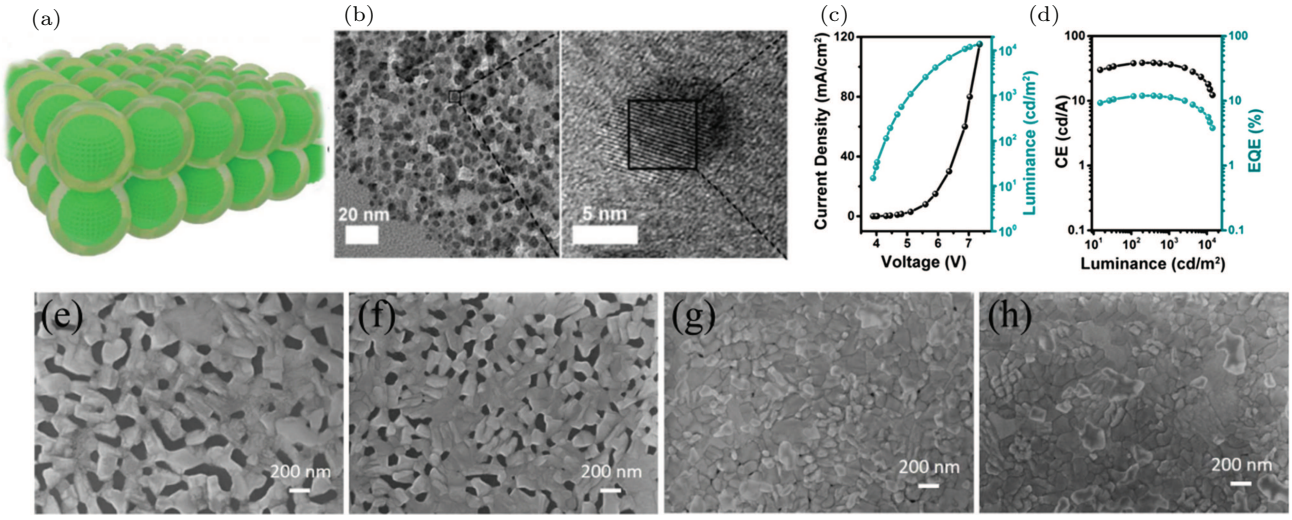


Fig. 8. (a) A schematic diagram of compositional feature of $CsPbBr_3$ SCQDs film;[70] (b) low resolution TEM image and high resolution TEM images of a typical $CsPbBr_3$ QD;[70] (c) *I*–*V*–*L* curves; (d) CE and EQE curves of the flexible large-area device;[70] top-view SEM images measured for the $CsPbBr_3$ perovskite layers grown on the ITO/PEDOT:PSS surface using (e) a pure $CsPbBr_3$ precursor solution, mixture solutions of (f) $CsPbBr_3$-Cs_2CO_3; (g) $CsPbBr_3$-PEO, and (h) a $CsPbBr_3$ precursor solution with a hybrid additive of PEO and Cs_2CO_3.[71]

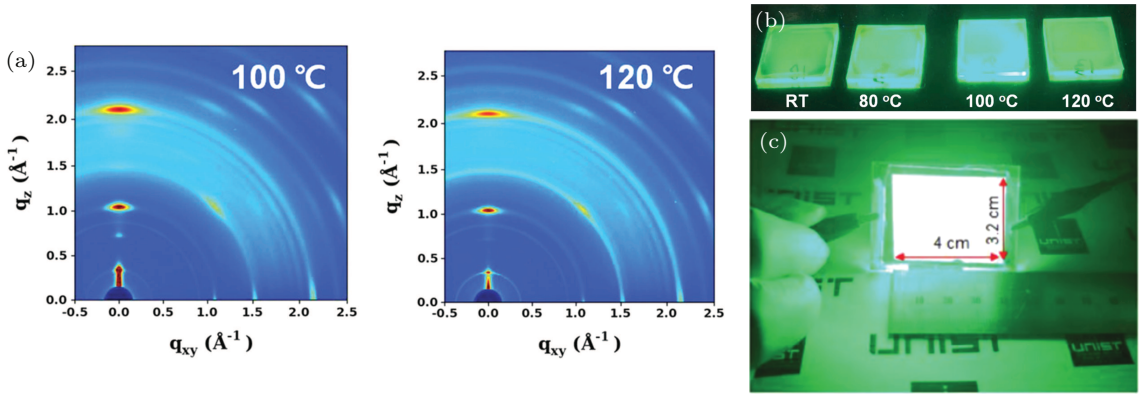


Fig. 9. (a) GIWAXS patterns of perovskite films fabricated at different substrate temperatures;[60] (b) photographs of perovskite films fabricated at different substrate temperatures under ultraviolet lamp illumination (375 nm);[60] (c) photograph showing EL emission of a large-area (1280 mm^2) PeLED fabricated by hot-casting method.[60]

Substrate preheating (hot casting) was used in spin-coating techniques to manufacture large-area PeSCs.[72] Hot casting decreases the surface tension between the perovskite precursor solution and bottom substrate, thereby facilitating the growth of spatially homogeneous and large-area perovskite films. In 2020, Song and co-workers developed an efficient and large-area PeLED by employing a hot casting method.[60] In this device, PVK was utilized as an interlayer, which increased the depth of the valence band maximum of NiO_x (from 5.1 eV to 5.5 eV), resulting in efficient hole injection. The temperature effect on the perovskite crystal was investigated by carrying out grazing-incidence wide-angle x-ray scattering (GIWAXS) (Fig. 9(a)). The room-temperature-cast management presented ring-like Debye–Scherrer patterns, which indicated a randomly oriented crystal. As a comparison, the hot-cast films showed a preferential face-on orientation of the substrate, clearly exhibiting discrete Bragg spots. Moreover, the x-ray diffraction (XRD) scattering intensities of the hot-cast

films were apparently observed to be higher than those of the room-temperature-cast film, indicating that the heating facilitated the growth of perovskite crystals. The optimized temperature of 100 °C showed the higher crystallinity of the hot-cast films. Furthermore, the optimal hot-cast film showed a highest photoluminescence intensity than the perovskite films grown at other handling temperatures, indicating that the hot-cast film grown at 100 °C showed the reduced trap-mediated non-radiative recombination, which might be attributed to optimized morphologies and crystallinity of hot-cast films. Figure 9(b) presented the photographs of the room-temperature-cast and hot-cast films under ultraviolet lamp illumination at 375 nm. It was apparent that the hot-cast film grown at 100 °C exhibited the strongest green emission. The high PLQY of the perovskite film under the optimal preheating temperature led to improved EL performance. The optimized PeLEDs (active area = 126 mm^2) showed an EQE of 3.6%, and the development of uniform and large-area (1280 mm^2) PeLEDs was demonstrated (Fig. 9(c))).

In the same year, Yang *et al*. demonstrated a 400-mm^2 green PeLED with high efficiency (EQE > 16%).[73] $FAPbBr_3$ nanocrystalline and poly(4-butylphenyl-diphenylamine) (poly-TPD) were employed as emission layer and HTL of PeLEDs, respectively (Fig. 10(a)). They reported a molecular modification strategy of a thin layer with 1,3,5-tris(bromomethyl) benzene (TBB), which was applied on poly-TPD to control the dynamics of film formation and passivate defects of emission layer by incorporating Br species. A smooth, dense emission layer was easily obtained in the large-area PeLEDs. As illuminated in Fig. 10(b), when the perovskite nanocrystal dispersion was spin-casted onto the TBB-coated poly-TPD, a uniform and densely-packed perovskite nanocrystal film was formed. As a result, the photoluminescence intensity of perovskite nanocrystal films was enhanced with adding TBB on the poly-TPD layer. Besides, the maximum EQE of PeLEDs with a TBB interlayer remained high as the active area increased from 100 mm^2 to 400 mm^2 (Fig. 10(c)). This could be explained by the passivation arising from TBB on perovskite nanocrystals, which led to the enhanced efficiency of the PeLEDs.

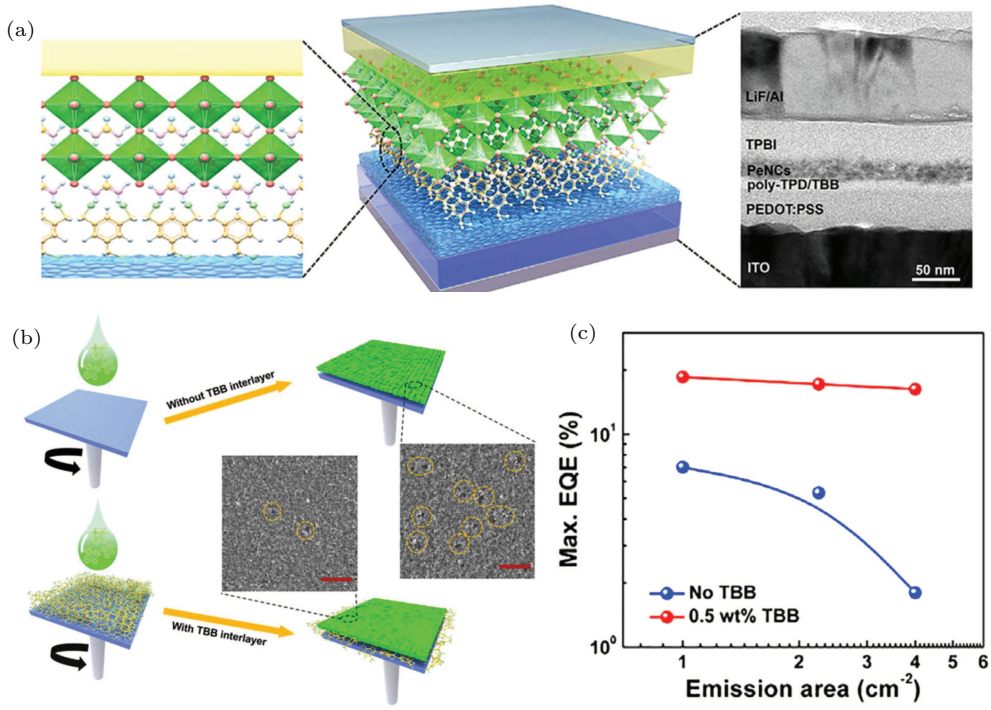


Fig. 10. (a) Device architecture and cross-sectional TEM image of the PeLEDs;[73] (b) deposition of perovskite nanocrystal solutions on poly-TPD and poly-TPD modified by TBB. All scale bars are 500 nm;[73] (c) the maximum EQE of PeLEDs with TBB (0.5 wt%) interlayer and without TBB interlayer on different device emission areas.[73]

Tan and co-workers fabricated the $FAPbI_3$-based PeLED with a structure of ITO/ZnO/ ethoxylated-polyethylenimine (PEIE)/$FAPbI_3$/poly-TPD/MoO_3/Al (Fig. 11(a)).[74] $FAPbI_3$ perovskite precursor was doped with 5-aminovaleric acid (5-AVA) as enhancement additive, which induced the formation of microstructure to improve the light extraction of PeLEDs.[75] They first demonstrated a 4-mm^2 PeLED, which showed a high radiance of 170 $W{\cdot}sr^{-1}{\cdot}m^{-2}$ at a driving voltage of 4.0 V. A remarkably high EQE of 20.2% was obtained at a high radiance of 57 $W{\cdot}sr^{-1}{\cdot}m^{-2}$ (Fig. 11(b)). And then, they manufactured a large-area of 900-mm^2 PeLED on a glass substrate. The NIR photograph of the device exhibited the remarkably uniform light emission across the entire device area (Fig. 11(c)). The device still showed a high radiance of near 30 $W{\cdot}sr^{-1}{\cdot}m^{-2}$ at a driving voltage of 4.0 V (Fig. 11(d)), and the efficiency remained apparently high at 12.1% under high-

radiance operation (> 20 W·sr^{-1}·m^{-2}). Besides, they also demonstrated a flexible 900-mm^2 PeLED with highest radiance of 0.56 W·sr^{-1}·m^{-2} (Figs. 11(e) and 11(f)). Compared to the rigid devices, the flexible device exhibited inferior performance, only 1.0% EQE. This may be attributed to the poor quality of the ITO layer and perovskite layer on the flexible PET substrate. The trend of large-area PeLEDs has become unstoppable.

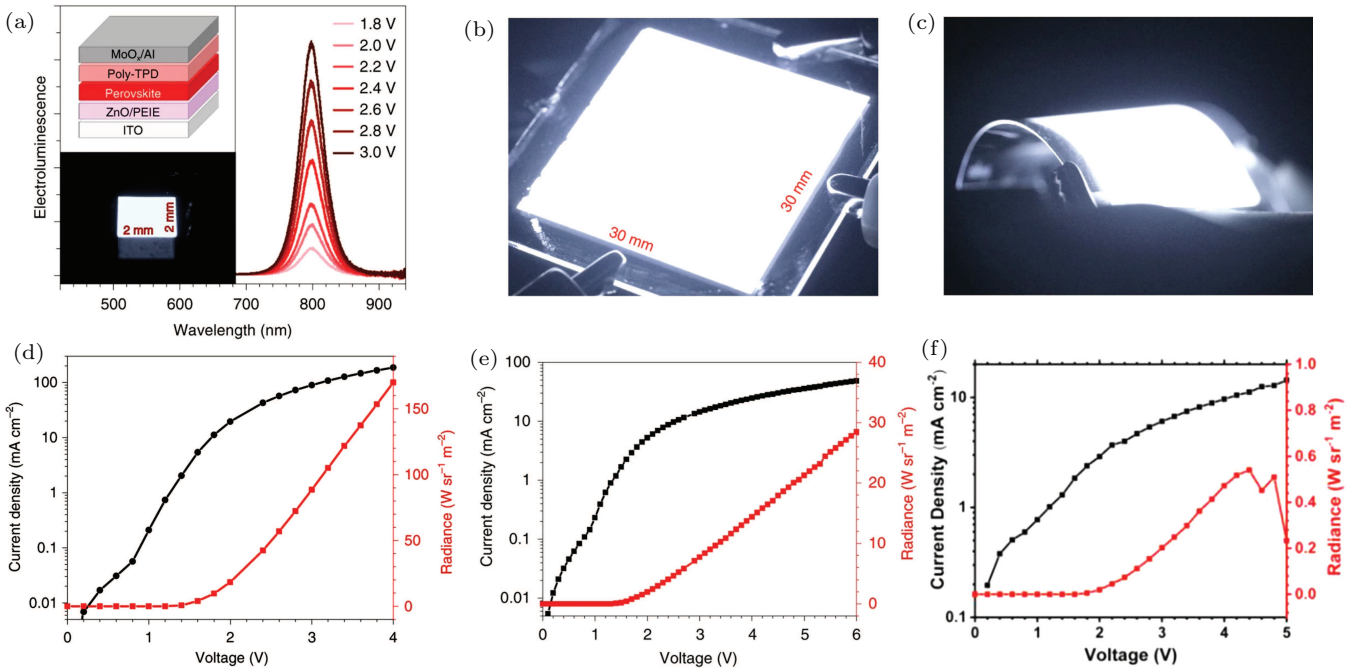


Fig. 11. Device characteristics of the PeLEDs.[74] (a) Device structure, EL spectra and NIR photograph of the 4-mm^2 PeLED; (b) combined current density *versus* voltage (black) and radiance *versus* voltage (red) plots of the 4-mm^2 PeLED; (c) NIR photographs of the 900-mm^2 PeLED on a glass substrate; (d) combined current density *versus* voltage (black) and radiance *versus* voltage (red) plots of the 900-mm^2 PeLED on a glass substrate; (e) NIR photographs of the 900-mm^2 PeLED on a flexible polyethylene terephthalate (PET) substrate; (f) combined current density *versus* voltage (black) and radiance *versus* voltage (red) plots of the 900-mm^2 PeLED on a flexible PET substrate.

6. Summary and outlook

In this paper, we primarily discussed the differences and similarities between manufacturing large-area PeLEDs and PeSCs, and introduced the technologies of fabricating large-area perovskite emission layers. Further, we illustrated the influence of CTLs and electrodes on the performances of large-area devices. Most importantly, we presented the progress of large-area PeLEDs (active area ≥ 30 mm^2) reported recently, and summarized the methods for achieving large-area PeLEDs in the literature.

Up till now, although there is significant progress in large-area PeLEDs, the necessary efforts are expected to realize the commercial manufacture of PeLEDs. Primarily, for large-area PeLEDs, the EQE of green and NIR devices are not more than 16.3% (active area = 400 mm^2) and 12.1% (active area = 900 mm^2), respectively. It is found in Table 1 that spin coating is the primary approach of fabricating large-area PeLEDs. Yet, the significant shortcomings in one-step spin coating have been summed up. Slot-die coating, spray coating, and CVD, *etc*. show the advantages of easy large-scale production, low material consumption, rapid manufacturing and controllable shape, which are significant in industrial production of PeLEDs. At present, the efficiencies of the PeLEDs obtained by the these methods are relatively low, thus the fabrication of the large-area high-efficiency PeLEDs by the technologies is bound to be a hotspot in the future. Besides, the stability is another challenge that urgently requires to be explored. The half-lifetime (T_{50}) of PeLEDs is only hundreds of hours.[76,77] Factors affecting the stability of PeLEDs include: the unstable chemical composition of perovskite; the ion migration in perovskite; and the external environment such as water, oxygen, heat, and light. The environmental degradation of PeLEDs can be eliminated by developing some novel encapsulation technologies. Meanwhile, it is necessary to vary the composition, and select the appropriate HTL materials to avoid the thermal instability and ion migration in PeLEDs. Moreover, the large-area blue PeLEDs are the prerequisite for high-performed large-area white PeLEDs. The present researches focus on green devices,[68–70] and the blue device seems to be ignored, which is mainly attributed to the low luminescence efficiency because of the low PLQY and wide bandgap of blue emission materials.[78,79]

The toxic lead-based perovskites are unfriendly to the environment and dangerous to human health, which seriously hinders their commercial application. Many attempts (such as Sn, Bi, or Sb) have been conducted to synthesize lead-free perovskites.[80,81] However, lead-free perovskites generally exhibit poor stability and optical properties compared with

lead-based perovskites. Yuan and co-workers fabricated the $CsSnBr_3$-based PeLEDs with a maximum EQE of 0.34%.[82] The 2D $(C_{18}H_{35}NH_3)_2SnBr_4$ layered perovskite was employed as emission layer to fabricated the lead-free PeLEDs with the maximum luminance of only 350 $cd{\cdot}m^{-2}$.[83] Although current lead-free PeLEDs are not comparable to lead-based PeLEDs as the photoelectric performance is concerned, they are still perceived as the candidates to realize environmental friendly PeLEDs. As expected, more and more strategies are adopted to solve these scientific problems. Thus, we can realize the large-scale manufacture of high-efficiency PeLEDs in the earlier future.

References

[1] Li Z C, Chen Z M, Zou G R X, Yip H L and Cao Y 2019 *Acta Phys. Sin.* **68** 158505 (in Chinese)
[2] Richter J M, Abdi-Jalebi M, Sadhanala A, Tabachnyk M, Rivett J P H, Pazos-Outón L M, Godel K C, Price M, Deschler F and Friend R H 2016 *Nat. Commun.* **7** 13941
[3] Su H, Chen J, Qin J, Zhu K and Li G L 2020 *Appl. Opt.* **59** 7975
[4] Wang N, Cheng L and Ge R, *et al.* 2016 *Nat. Photon.* **10** 699
[5] Yuan M, Quan L N, Comin R, Walters G, Sabatini R, Voznyy O, Hoogland S, Zhao Y, Beauregard E M, Kanjanaboos P, Lu Z, Kim D H and Sargent E H 2016 *Nat. Nanotechnol.* **11** 872
[6] Sutherland B R and Sargent E H 2016 *Nat. Photon.* **10** 295
[7] Stranks S D and Snaith H J 2015 *Nat. Nanotechnol.* **10** 391
[8] Liu B, Wang L, Gu H, Sun H and Demir H V 2018 *Adv. Opt. Mater.* **6** 1800220
[9] Wu J L, Dou Y J, Zhang J F, Wang H R and Yang X D 2020 *Acta Phys. Sin.* **69** 018101 (in Chinese)
[10] Cho H, Wolf C, Kim J S, Yun H J, Bae J S, Kim H, Heo J M, Ahn S and Lee T W 2017 *Adv. Mater.* **29** 1700579
[11] Yettapu G R, Talukdar D, Sarkar S, Swarnkar A, Nag A, Ghosh P and Mandal P 2016 *Nano Lett.* **16** 4838
[12] Yin W J, Yang J H, Kang J, Yan Y and Wei S H 2015 *J. Mater. Chem. A* **3** 8926
[13] Zhang F, Zhong H, Chen C, Wu X G, Hu X, Huang H, Han J, Zou B and Dong Y 2015 *ACS Nano* **9** 4533
[14] Tan Z K, Moghaddam R S, Lai M L, Docampo P, Higler R, Deschler F, Price M, Sadhanala A, Pazos L M, Credgington D, Hanusch F, Bein T, Snaith H J and Friend R. H 2014 *Nat. Nanotechnol.* **9** 687
[15] Wang Q, Wang X, Yang Z, Zhou N, Deng Y, Zhao J, Xiao X, Rudd P, Moran A, Yan Y and Huang J 2019 *Nat. Commun.* **10** 5633
[16] Lin K, Xing J, Quan L N, Arquer F P G, Gong X, Lu J, Xie L, Zhao W, Zhang D, Yan C, Li W, Liu X, Lu Y, Kirman J, Sargent E H, Xiong Q and Wei Z H 2018 *Nature* **562** 245
[17] Chiba T, Hayashi Y, Ebe H, Hoshi K, Sato J, Sato S, Pu Y J, Ohisa S and Kido J 2018 *Nat. Photon.* **12** 681
[18] Xu W, Hu Q, Bai S, *et al.* 2019 *Nat. Photon.* **13** 418
[19] Qu Z H, Chu Z M, Zhang X W and You J B 2019 *Acta Phys. Sin.* **68** 158504 (in Chinese)
[20] Zhang L, Yang X, Jiang Q, Wang P, Yin Z, Zhang X, Tan H, Yang Y M, Wei M, Sutherland B R, Sargent E H and You J B 2017 *Nat. Commun.* **8** 15640
[21] Wu C, Zou Y, Wu T, Ban M, Pecunia V, Han Y, Liu Q, Song T, Duhm S and Sun B 2017 *Adv. Funct. Mater.* **27** 1700338
[22] Chen A, Wang P, Lin T, Liu R, Liu B, Li Q J and Liu B B 2021 *Chin. Phys. B* **30** 048506
[23] Li J, Bade S G R, Shan X and Yu Z 2015 *Adv. Mater.* **27** 5196
[24] Zhao C, Zhang D and Qin C 2020 *CCS Chem.* **2** 859
[25] Cho H, Kim Y H, Wolf C, Lee H D and Lee T W 2018 *Adv. Mater.* **30** e1704587
[26] Lu M, Zhang Y, Wang S, Guo J, Yu W W and Rogach A L 2019 *Adv. Funct. Mater.* **29** 1902008
[27] Jiang Q, Chu Z, Wang P, Yang X, Liu H, Wang Y, Yin Z, Wu J, Zhang X and You J 2017 *Adv. Mater.* **29** 1703852
[28] Whitaker J B, Kim D H, Larson B W, Zhang F, Berry J J, Hest M F A M and Zhu K 2018 *Sustainable Energy Fuels* **2** 2442
[29] Zhang Z Y, Xu L and Qi J J 2021 *Chin. Phys. B* **30** 038801
[30] Chen Y, Zhang L, Zhang Y, Gao H and Yan H 2018 *RSC Adv.* **8** 10489
[31] Zhao Y, Ma F, Gao F, Yin Z, Zhang X and You J 2020 *Photon. Res.* **8** A1
[32] Xing G, Wu B, Wu X, Li M, Du B, Wei Q, Guo J, Yeow E K L, Sum T C and Huang W 2017 *Nat. Commun.* **8** 14558
[33] Chen S, Liu Y, Xiao X, Yu Z, Deng Y, Dai X, Ni Z and Huang J 2020 *Joule* **4** 2661
[34] Liu Z, He T, Wang H, Jain S M, Liu K, Yang J, Zhang N, Liu H and Yuan M 2018 *J. Power Sources* **401** 303
[35] Wang Z, Wang F, Sun W, Ni R, Hu S, Liu J, Zhang B, Alsaed A, Hayat T and Tan Z 2018 *Adv. Funct. Mater.* **28** 1804187
[36] McMeekin D P, Wang Z, Rehman W, Pulvirenti F, Patel J B, Noel N K, Johnston M B, Marder S R, Herz L M and Snaith H J 2017 *Adv. Mater.* **29** 1607039
[37] Park M H, Park J, Lee J, So H S, Kim H, Jeong S H, Han T H, Wolf C, Lee H, Yoo S and Lee T W 2019 *Adv. Funct. Mater.* **29** 1902017
[38] Xiao Z, Dong Q, Bi C, Shao Y, Yuan Y and Huang J 2014 *Adv. Mater.* **26** 6503
[39] Wu C, Zou Y, Wu T, Ban M, Pecunia V, Han Y, Liu Q, Song T, Duhm S and Sun B 2017 *Adv. Funct. Mater.* **27** 1700338
[40] Chen P, Xiong Z, Wu X, Shao M, Meng Y, Xiong Z H and Gao C 2017 *J. Phys. Chem. Lett.* **8** 3961
[41] Jeon S, Zhao L, Jung Y J, Kim J W, Kim S Y, Kang H, Jeong J H, Rand B P and Lee J H 2019 *Small* **15** 1900135
[42] Cheng G, Liu Y, Chen T, Chen W, Fang Z, Zhang J, Ding L, Li X, Shi T and Xiao Z 2020 *ACS Appl. Mater. Interfaces* **12** 18084
[43] Cheng L, Huang J S, Shen Y, Li G P, Liu X K, Li W, Wang Y H, Li Y Q, Jiang Y, Gao F, Lee C S and Tang J X 2019 *Adv. Opt. Mater.* **7** 1801534
[44] Zhao L, Lee K M, Roh K, Khan S U Z and Rand B P 2019 *Adv. Mater.* **31** 1805836
[45] Chih Y K, Wang J C, Yang R T, Liu C C, Chang Y C, Fu Y S, Lai W C, Chen P, Wen T C, Huang Y C, Tsao C S and Guo T F 2016 *Adv. Mater.* **28** 8687
[46] Cho H, Jeong S H, Park M H, Kim Y H, Wolf C, Lee C L, Heo J H, Sadhanala A, Myoung N, Yoo S, Im S H and Lee T W 2015 *Science* **350** 1222
[47] Ban M, Zou Y, Rivett J P H, Yang Y, Thomas T H, Tan Y, Song T, Gao X, Credington D, Deschler F, Sirringhaus H and Sun B 2018 *Nat. Commun.* **9** 3892
[48] Shen Y, Cheng L P, Li Y Q, Li W, Chen J D, Lee S T and Tang J X 2019 *Adv. Mater.* **31** 1901517
[49] Leyden M R, Meng L, Jiang Y, Ono L K, Qiu L, Juarez-Perez E J, Qin C, Adachi C and Qi Y 2017 *J. Phys. Chem. Lett.* **8** 3193
[50] Du P, Li J, Wang L, Liu J, Li S, Liu N, Li Y, Zhang M, Gao L, Ma Y and Tang J 2019 *ACS Appl. Mater. Interfaces* **11** 47083
[51] Jia K, Song L, Hu Y, Guo X, Liu X, Geng C, Xu S, Fan R, Huang L, Luan N and Bi W 2020 *ACS Appl. Mater. Interfaces* **12** 15928
[52] Derue L, Olivier S, Tondelier D, Maindron T, Geffroy B and Ishow E 2016 *ACS Appl. Mater. Interfaces* **8** 16207
[53] Choi K J, Lee J Y, Park J and Seo Y S 2015 *Org. Electron.* **26** 66
[54] Prakasam V, Tordera D, Giacomo F D, Abbel R, Langen A, Gelinck G and Bolink H J 2019 *J. Mater. Chem. C* **7** 3795
[55] Bade S G R, Li J, Shan X, Ling Y, Tian Y, Dilbeck T, Besara T, Geske T, Gao H, Ma B, Hanson K, Siegrist T, Xu C and Yu Z 2016 *ACS Nano* **10** 1795
[56] Park M, Cho W, Lee G, Hong S C, Kim M, Yoon J, Ahn N and Choi M 2019 *Small* **15** 1804005
[57] Karunakaran S K, Arumugam G M, Yang W, Ge S, Khan S N, Lin X, Yang G 2019 *J. Mater. Chem. A* **7** 13873
[58] Wang J, Wang N, Jin Y, Si J, Tan Z K, Du H, Cheng L, Dai X, Bai S, He H, Ye Z, Lai M L, Friend R H and Huang W 2015 *Adv. Mater.* **27** 2311
[59] Xu Y, Zhang Y T, Kou Z Q, Cheng S and Bu S L 2016 *Chin. Phys. Lett.* **33** 048501
[60] Kim D B, Lee S, Jang C H, Park J H, Lee A and Song M H 2020 *Adv. Mater. Interfaces* **7** 1902158
[61] Acik M, Lee G, Mattevi C, Chhowalla M, Cho K and Chabal Y J 2010 *Nat. Mater.* **9** 840
[62] Seo H K, Kim H, Lee J, Park M H, Jeong S H, Kim Y H, Kwon S J, Han T H, Yoo S and Lee T W 2017 *Adv. Mater.* **29** 1605587

[63] Zhang Q, Yu H, Liu Z, Lu Y, Ye D, Qian J, Wu Y, Gu W, Ma B, Zhang L, Duan Y, Liu L, Cao K, Chen S and Huang W 2019 *RSC Adv.* **9** 20931
[64] Park J W, Shin D C and Park S H 2011 *Semicond. Sci. Technol.* **26** 034002
[65] Le Q V, Jang H W and Kim S Y 2018 *Small Methods* **2** 1700419
[66] Kim H P, Kim J, Kim B S, Kim H M, Kim J, Yusoff A R, Jang J and Nazeeruddin M K 2017 *Adv. Opt. Mater.* **5** 1600920
[67] Kumar S, Jagielski J, Kallikounis N, Kim Y H, Wolf C, Jenny F, Tian T, Hofer C J, Chiu Y C, Stark W J, Lee T W and Shih C J 2017 *Nano Lett.* **17** 5277
[68] Yu M, Yi C, Wang N, Zhang L, Zou R, Tong Y, Chen H, Cao Y, He Y, Wang Y, Xu M, Liu Y, Jin Y, Huang W and Wang J 2018 *Adv. Opt. Mater.* **7** 1801575
[69] Kumar S, Jagielski J, Tian T, Kallikounis N, Lee W C and Shih C J 2019 *ACS Energy Lett.* **4** 118
[70] Yuan S, Wang Z K, Zhuo M P, Tian Q S, Jin Y and Liao L S 2018 *ACS Nano* **12** 9541
[71] Lau Y S, Lan Z, Li N and Zhu F 2020 *ACS Appl. Electron. Mater.* **2** 1113
[72] Liao H C, Guo P, Hsu C P, Lin M, Wang B, Zeng L, Huang W, Soe C M M, Su WF, Bedzyk M J, Wasielewski M R, Facchetti A, Chang R P H, Kanatzidis M G and Marks T J 2017 *Adv. Energy Mater.* **7** 1601660
[73] Wang H, Gong X, Zhao D, Zhao Y B, Wang S, Zhang J, Kong L, Wei B, Quintero-Bermudez R, Voznyy O, Shang Y, Ning Z, Yan Y, Sargent E H and Yang X 2020 *Joule* **4** 1977
[74] Zhao X and Tan Z K 2020 *Nat. Photon.* **14** 215
[75] Cao Y, Wang N, Tian H, *et al.* 2018 *Nature* **562** 249
[76] Wang H, Zhang X, Wu Q, Cao F, Yang D, Shang Y, Ning Z, Zhang W, Zheng W, Yan Y, Kershaw S V, Zhang L, Rogach A L and Yang X 2019 *Nat. Commun.* **10** 1
[77] Zhang L, Yuan F, Xi J, Jiao B, Dong H, Li J and Wu Z 2020 *Adv. Funct. Mater.* **30** 2001834
[78] Kumawat N K, Liu X K, Kabra D and Gao F 2019 *Nanoscale* **11** 2109
[79] Duan C C, Cheng L, Yao Y and Zhu L 2019 *Acta Phys. Sin.* **68** 158503 (in Chinese)
[80] Pal J, Manna S, Monda A, Das S, Adarsh K V and Nag A 2017 *Angew. Chem., Int. Ed.* **129** 14375
[81] Volonakis G, Haghighirad A A, Milot R L, Sio W H, Filip M R, Wenger B, Johnston M B, Herz L M, Snaith H J and Giustino F 2017 *J. Phys. Chem. Lett.* **8** 772
[82] Yuan F, Xi J, Dong H, Xi K, Zhang W, Ran C, Jiao B, Hou X, Jen K Y and Wu Z 2018 *Physica Status Solidi RRL* **12** 1800090
[83] Zhang X, Wang C, Zhang Y, Zhang X, Wang S, Lu M, Cui H, Kershaw S V, Yu W W and Rogach A L 2019 *ACS Energy Lett.* **4** 242